



HAL
open science

Highly selective inhibition of myosin motors provides the basis of potential therapeutic application

Serena Sirigu, James Hartman, Vicente José Planelles-Herrero, Virginie Ropars, Sheila Clancy, Xi Wang, Grace Chuang, Xiangping Qian, Pu-Ping Lu, Edward Barrett, et al.

► To cite this version:

Serena Sirigu, James Hartman, Vicente José Planelles-Herrero, Virginie Ropars, Sheila Clancy, et al.. Highly selective inhibition of myosin motors provides the basis of potential therapeutic application. Proceedings of the National Academy of Sciences of the United States of America, 2016, 113 (47), <10.1073/pnas.1609342113>. <hal-04041234>

HAL Id: hal-04041234

<https://hal.science/hal-04041234v1>

Submitted on 23 Mar 2023

HAL is a multi-disciplinary open access archive for the deposit and dissemination of scientific research documents, whether they are published or not. The documents may come from teaching and research institutions in France or abroad, or from public or private research centers.

L'archive ouverte pluridisciplinaire **HAL**, est destinée au dépôt et à la diffusion de documents scientifiques de niveau recherche, publiés ou non, émanant des établissements d'enseignement et de recherche français ou étrangers, des laboratoires publics ou privés.



HAL Authorization

Highly selective inhibition of myosin motors – the basis of potential therapeutic application

S. Sirigu^{1,2#}, J. Harman^{3#}, V.J. Planelles-Herrero^{1,2#}, V. Ropars^{1,2}, S. Clancy³, X. Wang³, G. Chuang³, X. Qian³, P. Lu³, E. Barrett⁴, K. Rudolph⁴, C. Royer⁴, B. Morgan³, E.A. Stura⁵, F.I. Malik³, A. Houdusse^{1,2*}

¹ Structural Motility, Institut Curie, PSL Research University, CNRS, UMR 144, F-75005, Paris, France. ² Sorbonne Universités, UPMC Univ Paris06, Sorbonne Universités, IFD, 4 Place Jussieu, 75252 PARIS cedex 053 Preclinical Research and Development, Cytokinetics, Inc., South San Francisco, CA 94080, USA. ⁴ Lovelace Respiratory Research Institute, 2425 Ridgecrest Dr. SE, Albuquerque, NM 87108-5127, USA. ⁵ CEA, DSV, iBiTec-S, Service d'Ingénierie Moléculaire des Protéines, 91191 Gif-sur-Yvette, France. #co-first authors

Submitted to Proceedings of the National Academy of Sciences of the United States of America

Direct inhibition of smooth muscle myosin (SMM) is a potential means to treat hypercontractile smooth muscle diseases. The selective inhibitor, CK-2018571, prevents strong binding to actin and promotes muscle relaxation in vitro and in vivo. The crystal structure of the SMM/drug complex reveals that CK-2018571 binds to a novel allosteric pocket that opens up during the “recovery stroke” transition necessary to reprime the motor. Trapped in an intermediate of this fast transition, SMM is inhibited with high selectivity compared to skeletal muscle myosin (IC₅₀ = 9 nM and 11,300 nM, respectively) although all of the binding site residues are identical in these motors. This structure provides a starting point from which to design highly specific myosin modulators to treat several human diseases. It further illustrates the potential of targeting transition intermediates of molecular machines to develop exquisitely selective pharmacological agents.

Myosin | Actin | Drug design | Molecular Motor | Specific allosteric drugs

Introduction

Myosins comprise a family of ATP-dependent motor proteins capable of producing directed force *via* interaction with their track, the F-actin filament. Force production by these motors powers numerous cellular processes such as muscle contraction, intracellular transport, cell migration and division¹. Several myosins have also been linked to genetic disorders where either gain or loss of motor function can lead to disease. These motor proteins represent promising targets for the development of drugs modulating force production in cells, tissues and muscle^{2,3,4}. Here we report the first selective, small-molecule inhibitor of smooth muscle myosin able to induce muscle relaxation. This mechanism of action has potential relevance for many diseases where smooth muscle contractility is central to the pathophysiology, such as asthma^{5,6} and chronic obstructive pulmonary disease⁷.

Smooth muscle contractility can be activated through different pathways. Existing airway smooth muscle relaxants, such as β -adrenergic agonists and muscarinic antagonists, ultimately inhibit the activity of smooth muscle myosin (SMM). However, they do so via specific upstream signalling pathways. Direct inhibition of SMM contractility has the advantage of relaxing contracted smooth muscle regardless of the molecular stimulus driving it. Moreover, application of SMM inhibitors to the airway provides a means of selectively modulating contractility of these tissues by delivering a high local concentration of drug. We thus set about identifying selective inhibitors of SMM that can effectively relax muscle *in vivo*, leading to the discovery of a highly selective, small molecule inhibitor, CK-2018571 (CK-571).

The detailed inhibitory mechanism of CK-571 was elucidated by a combination of *in vitro* characterization of the step in which the drug traps the motor and determination of the high resolution structure of SMM cocrystallized with CK-571. The drug targets an intermediate state that occurs during the recovery stroke, the large conformational rearrangement that enables repriming of

the motor. Blocking this critical transition thus results in efficient inhibition of force production. The SMM/CK-571 structure not only reveals how the drug stops the motor but also provides important insights about drug specificity. Our study establishes that the drug works via a new inhibitory mechanism that has *not been previously described for a molecular motor*, revealing a potentially powerful therapeutic approach for certain human diseases.

Results

Characterization of a highly selective smooth muscle myosin inhibitor, CK-571

Muscle contraction is powered by the myosin molecular motor that produces force during its powerstroke (Fig.1a). To promote tissue relaxation, inhibitors must stabilize myosin conformations that interact weakly with actin (Fig.1a). High throughput screens against smooth muscle myosin (SMM) and extensive medicinal chemical optimization led to compound CK-2018571 (CK-571). As shown in Fig.1b, the actin-activated ATPase of SMM is reduced to background levels in the presence of saturating concentrations of CK-571. The basal ATPase activity of SMM is also reduced more than 30 times upon CK-571 binding (Fig.1c). Interestingly, the compound displays an IC₅₀ of ~9 nM and a high degree of selectivity for SMM compared with cardiac and striated muscle myosins, for which the IC₅₀ is 280 and 1,255 fold lower,

Significance

Defects in myosin function are linked to a number of widespread and debilitating diseases, including asthma, chronic obstructive pulmonary disease and hypertrophic cardiomyopathy. We report here the discovery of an allosteric site that modulates myosin motor function with high specificity that opens the path towards new therapeutic solutions. Identification of specific anti-myosin drugs that significantly alter a motor's function is an imperative first step towards the development of highly targeted and effective treatments for such diseases. Highly specific drugs against different members of the superfamily would also provide exquisite tools to investigate in cells their functional role. Additionally, detailed, high-resolution studies of the interaction of drugs with their myosin target provide new insights into the molecular mechanism of motor function.

Reserved for Publication Footnotes

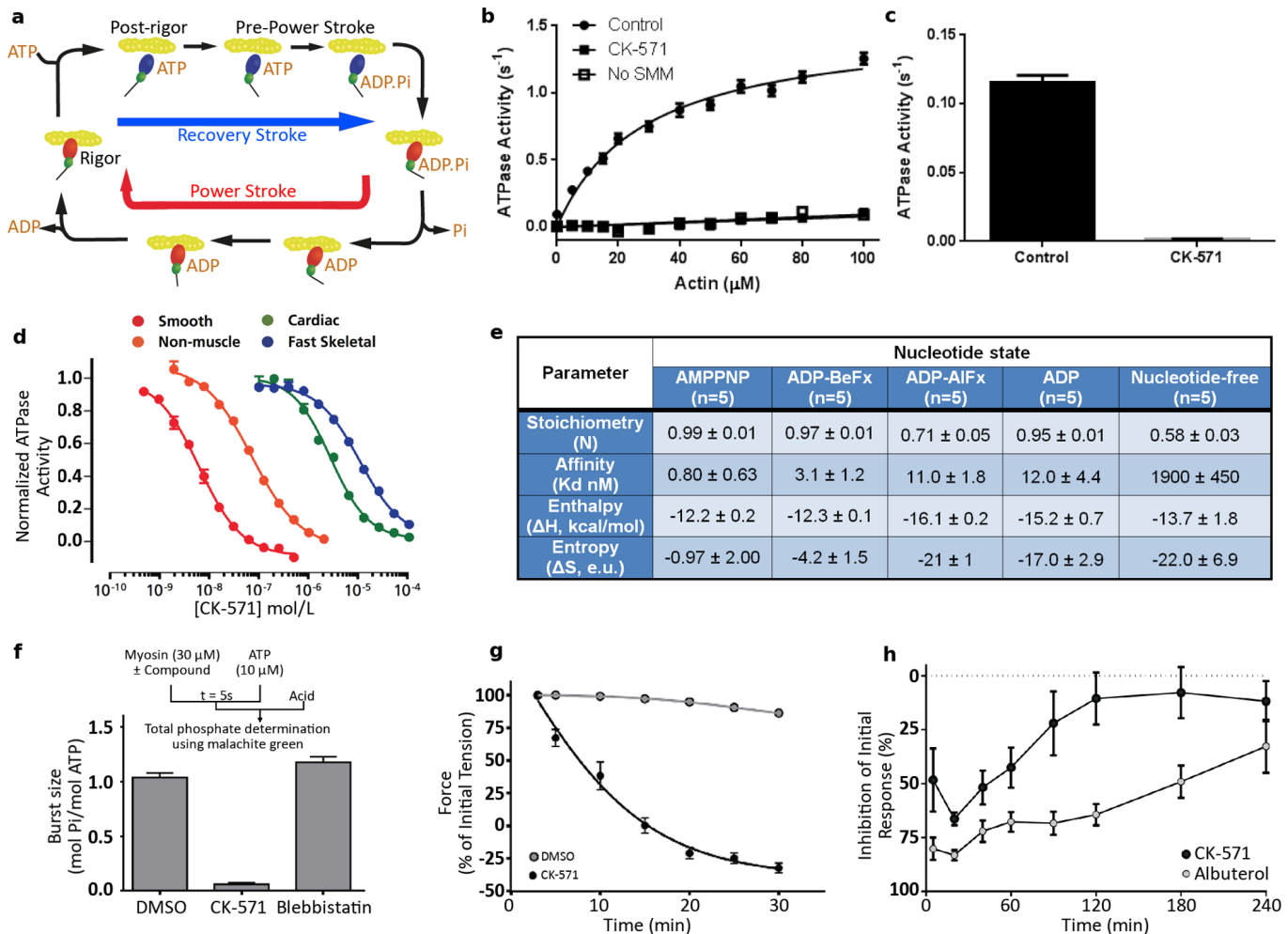


Fig. 1. Identification of a specific smooth muscle myosin inhibitor. (a) Chemo-mechanical cycle of myosin. Myosin motors generate force upon releasing hydrolysis products when attached to F-actin (Powerstroke, red arrow). A swing of the distal region of the motor, the lever arm, is associated with force generation. At the end of the stroke, nucleotide-free myosin is strongly attached to F-actin (Rigor). Myosin detaches from the filament upon ATP binding (Post-rigor, PR) and then undergoes transitions that reprime the lever arm during the recovery stroke (blue arrow). Hydrolysis stabilizes the Pre-powerstroke state (PPS). Rebinding to F-actin in the PPS state triggers a series of conformational changes associated with force production that also trigger Pi and ADP release (Powerstroke, red arrow). (b) Inhibition of theactin-activated ATPase of chicken gizzard SMM S1 ($0.35 \mu M$) by $5 \mu M$ CK-571 ($n=6$). Control reaction (2% DMSO) fit to a K_M of $29 \mu M$ and V_{Max} of $1.5 s^{-1}$ (Data are mean \pm SEM for $n=6$). (c) The basal ATPase of chicken gizzard SMM S1 ($1.8 \mu M$) is reduced from 0.12 ± 0.0036 to 0.0013 ± 0.00032 (mean \pm SD, $n=6$) by $25 \mu M$ CK-571. (d) CK-571 specifically inhibits the steady-state actin-activated MgATPase activity of SMM over other Myosin II isoforms. (IC50 \pm SD from triplicate samples: Smooth 9.0 ± 4.8 nM, Non-muscle IIB 76 ± 4.9 nM, Cardiac 2600 ± 240 nM, Fast skeletal 11300 ± 840 nM). (e) CK-571 binding to SMM is nucleotide-dependent and is stronger in the presence of AMPPNP in the binding pocket (f) CK-571 inhibits ATP hydrolysis as indicated by the reduced phosphate burst size in single turnover chemical quench experiments (mol Pi/mol myosin \pm SD from 5-10 samples: DMSO 1.04 ± 0.043 , CK-571 0.06 ± 0.016 , blebbistatin 1.18 ± 0.05). (g) CK-571 relaxes smooth muscle independent of calcium activation, as shown by the ability to relax skinned tailartery rings preactivated by thiophosphorylation ($n=8-12$, plotted is mean \pm SEM). (h) CK-571 relaxes airway smooth muscle *in vivo*, inhibiting methacholine-induced bronchoconstriction in naïve dogs following dry powder insufflation ($100 \mu g/kg$). For comparison, the clinically relevant β_2 -adrenergic agonist albuterol was dosed by nebulization ($10 \mu g/kg$). (Data are mean \pm SEM, $n=4$).

respectively (Fig.1d). Notably, CK-571 also has a significantly lower affinity for non-muscle myosins (NMMII, ~ 8.5 -fold less), which is remarkable given their high sequence homology to SMM (Supplementary Fig.1).

A major conformational change, the powerstroke, occurs when myosin is strongly bound to actin and drives the swing of the myosin lever arm during force production (Fig.1a). The myosin motor cycle also has states (blue, Fig.1a) of low affinity for actin when ATP is bound. While populating these states, the lever arm undergoes a recovery stroke to prepare the motor for producing force upon actin re-binding. As shown below, a series of *in vitro* assays established that CK-571 traps myosin in one of the ATP-bound intermediates of the recovery stroke in which the motor is dissociated from actin. Indeed, we show that the drug binds to a state of low affinity for actin (Supplementary Fig.2a)

with minimal effect on ATP binding to nucleotide-free actin-bound SMM (Supplementary Fig. 2b). CK-571 binds to myosin with highest affinity in the presence of the non-hydrolyzable ATP analogs AMPPNP (0.8 ± 0.63 nM) or ADP·BeFx (3.1 ± 1.2 nM), with somewhat weaker binding observed in the presence of ADP (12 ± 4.4 nM) or the ADP·Pi analog ADP·AlFx (11 ± 1.8 nM), (Fig.1e, Supplementary Fig.2b). The binding of nucleotide is critical for formation of a high affinity drug-myosin complex, as the affinity is decreased >2000 -fold in the absence of nucleotide (1900 ± 450 nM), (Fig.1e, Supplementary Fig.2g). AlFx, a Pi analog that promotes the formation of pre-powerstroke states (with ADP·Pi trapped), probably hinders CK-571 binding since the observed stoichiometry is only 0.71 and the apparent K_d is similar to that measured for ADP alone, i.e. 11 nM (Fig. 1e). Importantly, the drug also prevents ATP cleavage as shown by

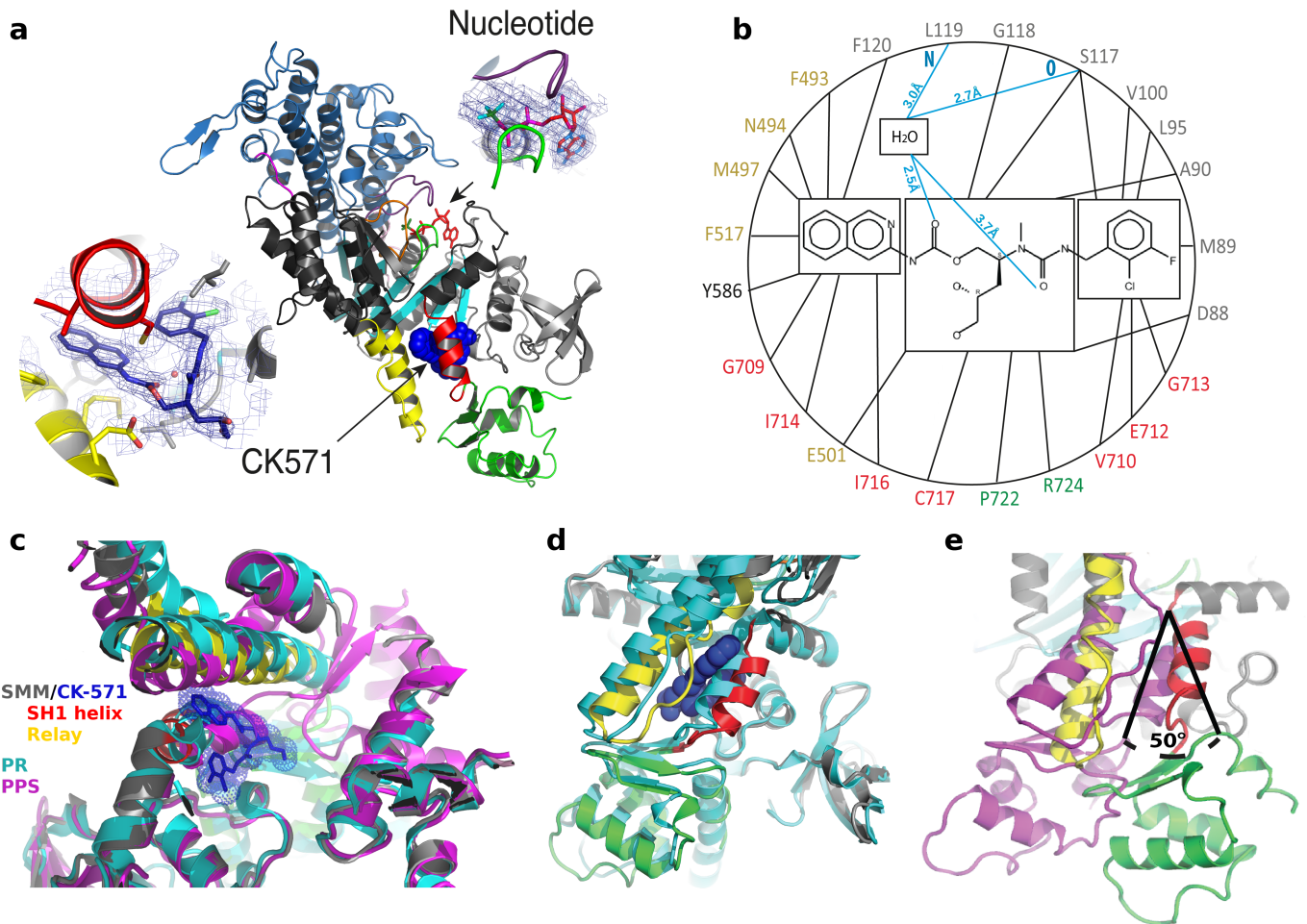


Fig. 2. An allosteric pocket opens to bind CK-571 during the recovery stroke. (a) Overall view of the myosin motor domain of the SM/CK-571 structure in cartoon representation. CK-571 is shown in blue spheres and is located 22 Å away from the nucleotide (right insert: red sticks, ADP; green sticks, BeFx). CK-571 (left insert: 2Fo-Fc electron density) interacts with residues of the SH1 helix (red), Relay (yellow) and the Nter subdomain (light grey) as well as with Y586 from the L50 subdomain (dark grey). The other two subdomains of the motor are the U50 (blue) and converter (green). (b) Residues of the CK-571 binding site (black lines, apolar contacts; blue lines, polar contacts). Residues are indicated with the same color code as in a. (c) Comparison of the CK-571 binding pocket with the myosin post-rigor (315F, PR, cyan) and pre-powerstroke (1BR1, PPS, magenta). Only the SH1 helix and the relay conformation in the SM/CK-571 structure are compatible with the drug binding. (d) Comparison of the SM/CK-571 structure with the myosin post-rigor state (315F, cyan). In the SM/CK-571 structure, rearrangements of the Relay (yellow) and a 10° rotation of the SH1 helix (red) allow the formation of a cleft in the molecule that harbors the drug (blue spheres). (e) In the SM/CK-571 structure, the converter is in a down position and is rotated by 50° with respect to the position it occupies in the pre-powerstroke state (1BR1, magenta). In order to compare the three structures, the proteins were aligned in (c), (d) and (e) using the N-ter domain as a reference.

quench flow experiments and reduced level of Pi burst (Fig. 1f, Supplementary Fig. 2c). This inhibitor thus traps the motor in an ATP state that cannot cleave ATP. CK-571 prevents completion of the recovery stroke and precludes the motor from forming states that would rebind to F-actin and produce force. By preventing the population of force generating states, CK-571 binding relaxes muscle *in vitro* and *in vivo* (Fig. 1g, 1h, Supplementary Fig. 2d). In summary, CK-571 binding traps myosin in a state that cannot bind strongly F-actin with ATP rather than ADP:Pi trapped in the active site (Fig. 1f). With CK-571, the absence of ATP cleavage and thus the absence of Pi possible to be released prevents productive actin association necessary for force production. This new mechanism of myosin inhibition, that stops the motor prior to ATP cleavage, differs drastically from those previously described for modulators of myosin activity such as blebbistatin (Fig. 1f) or *omecamtiv mecarbil* that are both compatible with the recovery-stroke. This mechanism is particularly efficient at preventing any productive interaction of the motor with the actin filament, precluding any force generation.

Relaxation of smooth muscle by CK-571

Therapeutically relevant SMM inhibitors must be able to promote tissue relaxation. Importantly, the inhibition of SMM-catalyzed ATP hydrolysis by CK-571 effectively relaxes smooth muscle tissue *in vitro* and *in vivo*. CK-571 inhibits force production in detergent-permeabilized skinned artery rings stimulated to contract by increasing concentrations of calcium in a dose-responsive fashion (Supplementary Fig. 2d,e). In addition, CK-571 promotes relaxation in thiophosphorylated skinned artery rings, demonstrating that the compound can relax pre-contracted tissue and supporting a direct effect on myosin rather than upstream signalling pathways acting through MLCK (Fig. 1g). CK-571 relaxes rat tracheal rings that have been pre-contracted with the muscarinic receptor agonist methacholine with similar potency, highlighting the ability of CK-571 to penetrate and relax intact smooth muscle tissue (Supplementary Fig. 2f). Relaxation of skinned and intact tissues requires higher concentrations (approximately μM), consistent with a need to inhibit >95% of the smooth muscle myosin to achieve relaxation. The therapeutic potential of this mechanism is further supported by the ability of CK-571 to inhibit methacholine-induced bronchoconstriction

409
410
411
412
413
414
415
416
417
418
419
420
421
422
423
424
425
426
427
428
429
430
431
432
433
434
435
436
437
438
439
440
441
442
443
444
445
446
447
448
449
450
451
452
453
454
455
456
457
458
459
460
461
462
463
464
465
466
467
468
469
470
471
472
473
474
475
476

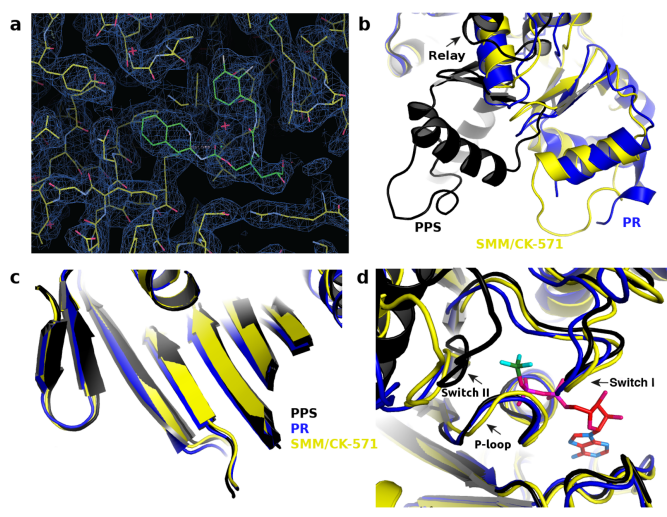


Fig. 3. Structural features of SMM2 motor domain in complex with CK-571 that traps an intermediate of the recovery stroke. (a) 2Fo-Fc electron density omit map, contoured at 0.7 σ , depicting the CK-571 binding site. (b) The SM-CK-571 is an intermediate between the Post-Rigor (PR, pre-recovery stroke) and Pre-powerstroke (PPS, post-recovery stroke) structures. Note in particular the difference in position of the converter in these structures, it is in a down position in the SM/CK-571 structure (yellow), close to the position found in the PR state structures (blue) and differs greatly from the up position found in PPS structures (black). The position of the subdomains when CK-571 is bound differs from those found in previously described PR structures. Interestingly, the relay (shown in this figure) and L50 subdomain (see Movie 3) corresponds to an intermediary position between the PR and the PPS structures. (c) The central beta sheet conformation (which is part of the transducer) controls rearrangements between subdomains of the motor1. While the lever arm position in SM/CK-571 is closer to the PR than the PPS position, the central beta sheet conformation of SM/CK-571 (yellow) differs from that of the PR state (blue) while its position is quite similar to that found in the PPS state (black) (Movie S3). (d) Nucleotide binding site in the SM/CK-571, PR and PPS structures. Note that the nucleotide binding elements Switch I and P-loop are in position to bind MgATP tightly. However in the SM/CK-571 structure, the Switch II position differs from the special PPS position necessary to promote ATP hydrolysis (black). This Switch II position is far away from the nucleotide, in an intermediate position between the PR and PPS states. (PPS, 1BR1, black; PR, 3I5F, blue; SM/CK-571 is in yellow with the nucleotide in red sticks).

in naïve dogs following dry powder delivery of CK-571 (achieved dose 100 μ g/kg). The magnitude of the inhibition achieved is comparable to the clinically relevant short-acting β 2-adrenergic agonist albuterol (Fig.1h). Given that CK-571 requires higher doses and has a shorter duration of action, potency and metabolic stability are key areas for further optimization.

Mechanism for this efficient and highly selective myosin inhibitor.

The structural basis of CK-571 action and specificity was revealed by the crystal structure of the SMM motor domain bound to CK-571 (SM/CK-571; PDB code: 5CK8) at 2.8 Å resolution (Supplementary Table 1). The electron density shows unambiguously that the inhibitor binds in an unexpected pocket of the motor domain (Fig.2a,3a). CK-571 is held in between two structural elements that control the lever arm position, the Relay and the SH1 helix (Fig.2a, Supplementary Movie 1), burying 1067 Å² of surface area in an internal pocket. It adopts a compact conformation in which the isoquinoline carbamate and the chloro-fluoro-phenyl moieties come close together via a ~60° bend in the central aliphatic chain of CK-571 (Fig.2a insert). The inhibitor has a predominant hydrophobic character and interacts via a complex network of mostly apolar contacts (Fig.2b). There are no direct H-bonds established with protein residues. Importantly, the drug binding site of CK-571 is not accessible in

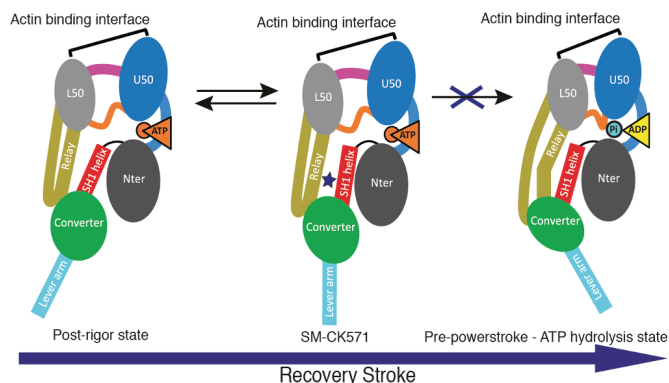


Fig. 4. Motor domain rearrangements upon the recovery stroke.The myosin motor domain is functionally made up of four subdomains linked by connectors that rapidly change their conformation upon transitions in the motor cycle. In particular, Switch II (orange) is found close to the nucleotide. The Relay (yellow) and the SH1-helix (red) connect the motor domain to the converter (green) and controls its swing. The converter and the adjacent neck region constitute the lever arm that amplifies motor domain rearrangements linked to nucleotide or actin binding. Binding of CK-571 (blue star) blocks the motor isomerization in an intermediate of the recovery stroke. Thus, unlike prevailing models, lever arm repriming corresponds to an uncoupling of these connectors and lead to transducer rearrangements that are not initiated by a Switch II closure. Lever arm swing in this step is not controlled by mechanical control of subdomain orientation by coupled connectors.

either the Post-rigor or the Pre-powerstroke states (Fig.2c,2d) since the Relay and the SH1 helix make strong interactions in these two structural states that correspond to the beginning and the end of the recovery stroke. These structural insights and the functional studies presented above (that show that ATP binding is not affected by CK-571 while ATP cleavage cannot occur) show that CK-571 binds a myosin-ATP intermediate that is populated during the recovery stroke. Thus, a pocket between the Relay and the SH1 helix must open during this transition. Once bound, CK-571 traps the motor in an intermediate state which prevents the motor from exploring states at the end of the recovery stroke that are necessary for ATP hydrolysis. Small angle X-ray scattering (SAXS) studies were performed to demonstrate that the X-ray SM/CK-571 structure corresponds to the state populated by the drug in solution. The SMM motor with CK-571 and either ADP or ADP.BeFx bound adopt a similar conformation in solution, that also fits the scattering curve calculated from the SM/CK-571 structure (Supplementary Fig.3). In contrast, the scattering curve is quite different when SMM is in the pre-powerstroke state (PPS, with ADP.VO4 bound), confirming that the drug prevents access to PPS. Details of the structure compared to previously characterized ATP states prior or after the recovery stroke are shown in Figs.2c, 2d, 2e, 3. The intermediate state populated by CK-571 has similarities with the post-rigor state populated at the beginning of the recovery stroke because of the position of its lever arm (in the down position). However, other motor domain elements are more similar to the conformation myosin motors adopt at the end of the recovery stroke. In particular, the intermediate state trapped by CK-571 differs substantially from the post-rigor state since the central β -sheet of the motor domain in this intermediate adopts a conformation close to that found in states at the end of the recovery stroke (PPS, Fig.3c, Supplementary Movies 3,4). This β -sheet is a major part of the transducer¹ that coordinates several allosteric sites within the motor, in particular the actin-binding interface and the nucleotide binding site. Moreover, the Switch II element near the γ -phosphate of ATP has moved towards the conformation it adopts in the PPS state that allows direct interaction with the nucleotide necessary for hydrolysis. However, it remains far from this final conformation since it adopts

477
478
479
480
481
482
483
484
485
486
487
488
489
490
491
492
493
494
495
496
497
498
499
500
501
502
503
504
505
506
507
508
509
510
511
512
513
514
515
516
517
518
519
520
521
522
523
524
525
526
527
528
529
530
531
532
533
534
535
536
537
538
539
540
541
542
543
544

545 a position intermediate between the two end structures of the
546 recovery stroke (PR and PPS, **Fig.1a, Fig.3d**). This result indicates
547 that in contrast to what had been proposed from some Molecular
548 Dynamics simulations¹², sensing the nucleotide via switch II does
549 not correspond to the first event that would guide the repriming of
550 the lever arm. The recovery stroke of the lever arm is not driven by
551 keeping strong interactions between the Relay and SH1 helix, as
552 previously proposed¹². Indeed, this mechanism¹² cannot explain
553 how a pocket would open during the recovery stroke to allow CK-
554 571 binding. Overall, the SMM/CK-571 structure reveals that CK-
555 571 traps the motor in an intermediate state in which Switch II
556 stays too far from the nucleotide to stabilize the water near the
557 γ -phosphate that allows cleavage of ATP.

558 Intriguingly, sequence analysis reveals that all 24 residues
559 forming the inhibitor's binding site are strictly conserved among
560 SMM, NMM, fast skeletal and cardiac muscle myosin II, thus
561 indicating that the inhibitor's selectivity is not based on specific
562 sequence recognition at the drug site (**Fig.1d, Supplementary Fig.1**).
563 Furthermore, no sequence differences exist among the residues located
564 along the putative pathways by which the compound would reach this
565 site (**Supplementary Movie 2**). In summary, comparison of the SM/CK-
566 571 structure with other myosin II structures (**Supplementary Table 2**),
567 SAXS data as well as functional characterization of the motor inhibited
568 by CK-571 demonstrate that the drug traps myosin in an intermediate
569 ATP state of the recovery stroke incapable of ATP hydrolysis and thus
570 blocks the motor from cycling, killing force production (**Fig.4**).

571 **CK-571 reveals the existence of a novel allosteric pocket** 572 **adjacent to the binding site of the omecamtiv mecarbil myosin** 573 **activator.**

574 A structure of cardiac myosin II bound to the activator *ome-*
575 *camtiv mecarbil*² was recently solved⁸ with the motor in the post-
576 rigor state (PR, **Fig.1a**). This activator of cardiac myosin increases
577 force production by the heart by increasing the transition of cardiac
578 myosin from a weakly to strongly actin bound state as evidenced by a
579 faster rate of Pi release^{2,9} and by slowing down the following steps
580 of the powerstroke. In the crystal structure, *omecamtiv mecarbil*
581 binds to cardiac myosin⁸ in a surface pocket accessible in the post-
582 rigor state (**Fig.1a**). The *omecamtiv mecarbil* pocket only slightly
583 overlaps with the CK-571 pocket. Indeed most of the CK-571 site is
584 not accessible in the post-rigor state and opens up only during the
585 recovery stroke (**Fig.2c, Supplementary Fig.4**). The most deeply
586 buried *omecamtiv mecarbil* groups (carboxymethyl-piperazine and
587 fluoro-benzene rings) are located close to the SH1 helix where the
588 CK-571 binding site opens during the transition (**Supplementary Fig.4a**).
589 The rest of the *omecamtiv mecarbil* groups (amino-carbamoyl and
590 methyl-pyridinyl) are located closer to the surface of the molecule
591 near the converter domain. In contrast, the binding site shown for
592 CK-571 is much deeper and quite different from that of *ome-*
593 *camtiv mecarbil* (**Supplementary Fig.4**). It is unlikely that in fact
594 *omecamtiv mecarbil* would occupy the CK-571 pocket during the
595 recovery stroke. Unlike CK-571, *omecamtiv mecarbil* does not
596 block the motor in an intermediate of the recovery stroke but
597 increases the population of the end states of the recovery stroke
598 (Pre-powerstroke state), in which the lever arm is up. It must thus
599 occupy a pocket that is accessible in the pre-powerstroke state.
600 This is not the case for the CK-571 pocket which is non-existent
601 in the Pre-powerstroke state. In contrast to CK-571, *omecamtiv*
602 *mecarbil* is compatible with the recovery stroke, accelerates Pi
603 release and then slows the following steps of the powerstroke⁹.
604 Thus, cardiac muscle contracts more strongly when the drug is
605 present² and *omecamtiv mecarbil* acts as an activator of force
606 production. Together, the *omecamtiv mecarbil* and CK-571 binding
607 sites on myosin thus highlight the potential of targeting the
608 internal pockets found near the SH1 helix and the Relay to design

609 highly specific activators and inhibitors of myosin motors for the
610 treatment of numerous diseases in which myosin motors are a
611 target.

612 Discussion

613 The atomic structure of SM/CK-571 reveals that the drug binds
614 in a novel allosteric pocket of the myosin motor that opens up
615 transiently during the recovery stroke of the myosin motor.

616 The drug introduces itself in a pocket that has not been
617 found in the previously described structures of the motor. Fur-
618 thermore, this pocket becomes available transiently when the
619 ATP-bound motor explores states of the recovery stroke. The
620 intermediate state is then stabilized and traps the motor in a
621 phase of the recovery stroke from which myosin cannot bind
622 actin nor progress towards ATP hydrolysis. Drug binding blocks
623 the recovery stroke transition via stabilization of an intermediate
624 through interactions with two main connectors (Relay and SH1
625 helix) that link the motor and the lever arm. It thus prevents
626 the motor from reaching the states at the end of the recovery
627 stroke (pre-powerstroke state) that are required to allow ATP
628 cleavage. This efficiently blocks the motor in states that are
629 inappropriate for force production upon interaction with actin
630 since ATP is not cleaved, affinity for F-actin is low and the lever
631 arm is not primed. Previously described myosin inhibitors, such
632 as blebbistatin or pentabromopseudinin^{3,10,11}, trap the motor in
633 the pre-powerstroke state (PPS) at the beginning of the force
634 production event (**Supplementary Fig.4e**). These drugs do not
635 prevent ATP cleavage and bind surface pockets available in the
636 PPS state of cytoplasmic and muscle myosin II with lower affinity
637 and specificity¹² compared to CK-571. In contrast, stabilization
638 of an intermediate state during the recovery stroke by CK-571 not
639 only blocks the motor rearrangements required for lever arm
640 re-priming but also those needed for the closure of the nucleotide
641 binding site that are required for ATP hydrolysis. By keeping the
642 myosin heads away from any possible interaction with F-actin,
643 precluding ATP hydrolysis and re-priming of the lever, CK-571
644 prevents these heads from participating in force production. CK-
645 571 exemplifies an innovative and efficient mechanism to achieve
646 complete relaxation of smooth muscle.

647 Interestingly, all of the residues of the CK-571 binding pocket
648 are conserved among the different human myosin IIs (cytoplasmic,
649 smooth, skeletal and cardiac). Thus, the selectivity of CK-
650 571 must result from residues outside the binding pocket that
651 modulate the kinetics and energy landscape of the recovery stroke
652 (**Supplementary Fig.1**). What differs among myosins is the ability
653 of the drug to exploit a transient pocket formed during the
654 recovery stroke. These differences may arise from small sequence
655 changes between these molecular motors that influence the life-
656 times and the nature of the intermediate states. CK-571 inhibits
657 SMM2 with ~8-fold greater potency than its close homolog,
658 NMM, in spite of the lack of any sequence differences within
659 the drug binding pocket or any of the surrounding amino acids.
660 CK-571 provides a remarkable demonstration of the principle of
661 allosteric modulation of enzyme function by a small molecule with
662 high specificity and high affinity. The SMM-CK-571 structure
663 reveals a new way to achieving specificity by targeting transient
664 pockets likely to have different life times in different myosins
665 with sequence differences even remote from the drug binding
666 site. Even highly homologous Myosins can be specifically inhib-
667 ited as long as they have kinetics that differ significantly from
668 each other. The SM/CK-571 structure provides important insights
669 into the allosteric mechanism of the recovery stroke transition,
670 the critical step in which the ATP-bound motor, detached from
671 actin, primes its lever arm to prepare myosin for its powerstroke.
672 During this isomerization, the lever arm undergoes a drastic re-
673 orientation while the SH1 helix and Relay connectors explore dif-
674 ferent conformations. The trapped intermediate in the SM/CK-

571 structure sheds light on the recovery stroke mechanism, refuting models supporting tight coupling between the nucleotide binding site and the lever arm. Weak interactions between the Relay and SH1 helix are necessary for pocket opening and CK-571 binding. Models in which Switch II interactions with the nucleotide direct the swing of the converter through a strong coupling mechanism between the Relay and SH1 helix cannot explain how CK-571 may bind. Re-arrangements of the Relay and the SH1 helix during lever arm priming can allow the formation of a large pocket in between them, which traps the drug in place (**Supplementary Movies 1,3,4**). In the Rigor, PR and PPS states, (**Fig.1a**) these two connectors interact directly, preventing this pocket from being formed, thus precluding CK-571 binding.

Molecular simulations have provided drastically different models for the recovery stroke. A coupling mechanism discussed above in which the active site (Switch II closure) would trigger re-orientation of the converter is not compatible with the SM/CK-571 structure^{13,14}. In contrast, the structure is consistent with a Targeted Molecular Dynamics approach, in which the converter rotates in the first stage of the transition prior to Switch II closure^{15,16}. Transient time-resolved FRET data are also compatible with this scenario¹⁷ as are previous studies that indicate the potential melting of the SH1 helix in this transition^{18,19}. Furthermore, the SM/CK-571 structure shows that the lever arm repriming doesn't occur via Switch II sensing of the γ -phosphate. This structure reveals that the recovery stroke (a large 9 nm movement) necessary to reprime the motor is likely to capture thermal energy to explore and populate uncoupled states that allow a lever arm swing. This differs from mechanism in which such large movement would occur via the use of chemical energy linked to formation of bonds along a pathway from the active site to the lever arm that would trigger precise allosteric rearrangements to control lever arm movement. The emerging model of the recovery stroke thus differs greatly from current ones that suggest allosteric communication between the nucleotide binding site and a distal part of the motor to reprime the lever arm.

The recovery stroke is an essential step of the cycle of all myosins. Highly specific drugs that trap intermediates of this transition can thus be designed for other myosins on the basis of the SM/CK-571 structure. Structural studies with several myosins isoforms, and in particular the reverse motor Myosin VI have shown that the conformation of the motor in the states prior and after the recovery stroke are similar, even when the direction of the lever arm swing differs²⁰. Selectivity among different myosin classes may be achieved by exploiting sequence differences in the CK-571 binding pocket (**Supplementary Fig.5**). This allosteric binding site has thus the potential to guide the design of novel class-specific myosin inhibitors. In particular, myosin VI and myosin X are interesting pharmaceutical targets due to their recently established role in cell migration and metastasis²¹⁻²⁴.

METHODS

Crystal Structure determination:

Chemicals

CK-571 was synthesized by the Medicinal Chemistry group of Cytokinetix. Other chemicals were from commercial sources and generally ACS grade or higher.

High throughput screens were conducted using chemically-diverse libraries of commercially-available small molecules, resulting in the identification of an initial hit with modest biochemical potency (IC₅₀=17 μ M) against smooth muscle myosin. Through extensive medicinal chemical optimization (>3000-analogs in series) the intrinsic biochemical potency of the chemical series was greatly improved, resulting in an IC₅₀ of ~9 nM for compound CK-571. Inhibitors with higher selectivity for smooth muscle myosin (SMM) versus nonmuscle myosins (NMMs) were sought during optimization. A selectivity ratio of 10-20-fold was measured consistently across the chemical series (data not shown).

Purification of myosins

Native chicken smooth muscle myosin was purified from cryoground gizzards (Pel-Freez Biologicals) using previously described methods²⁵. Soluble chicken gizzard subfragment 1 (S1) was obtained by limited papain digestion

of filamentous myosin terminated with 1 mM iodoacetic acid. Recombinant chicken smooth muscle myosin motor domain²⁵ (MD, residues Met1-790) and motor domain + essential light chain (MDE heavy chain residues Met1-Leu819, Genbank NP.990605.2; Essential Light Chain M15645.1), were expressed with a C-terminal FLAG tag following a short linker (sequence: GSDYKDDDDK). The chicken MDE protein was prepared by co-expression of the untagged chicken essential light chain. Recombinant human smooth muscle myosin motor domain and essential light chain (MDE, heavy chain residues Met1-Leu820, isoform SM-A, Genbank NP.002465) was expressed with a C-terminal 6xHis tag. Human non-muscle myosin IIB and essential light chain (MDE, heavy chain residues Met1-Pro843, isoform 2, Genbank NP.005955.3) was expressed with a C-terminal FLAG tag (sequence: DYKDDDDK). The human MDE proteins were prepared by co-expression of the untagged human smooth muscle myosin essential light chain. The isoforms of the recombinant human smooth and nonmuscle myosins both lacked the 7 amino acid insert in loop 1, however the presence of this insert does not affect the IC₅₀ of CK-571 (data not shown). FLAG-tagged recombinant proteins were purified from baculovirus-infected SF9 cells by ammonium sulphate precipitation and affinity chromatography as described²⁶. Rabbit fast skeletal and bovine cardiac myosins were purified from native tissues (Pel-Freez Biologicals) and digested in their filamentous forms with chymotrypsin to produce S1 fragments²⁷. For measuring specificity and potency, soluble myosin fragments were covalently cross-linked to excess bovine cardiac actin using EDC/NHS^{28,29} and flash frozen at -80°C prior to use in ATPase assays.

Crystallization and structure determination

Purified chicken Smooth Muscle Myosin MD (residues 1-790) at 110 μ M was incubated with 2mM MgADP and 2 mM BeFx for 30 min on ice. The protein was mixed with CK-571 at final concentration of 547 μ M in the presence of 10% DMSO and then it was incubated for 1h on ice. Samples were centrifuged at 11,000 x g for 15 min before crystallization. Hanging drops of SM/CK-571 were set up by mixing equimolar ratio of the complex and of the reservoir containing 5% Peg8K, 50 mM Bicine pH 8.2, 10% DMSO. First crystals appeared after 10 days at 4°C and were subsequently optimized using micro-seeding technique. The optimized crystals were cryo-cooled in a final solution containing 8% Peg8K, 50 mM Bicine pH 8.2, 10% DMSO, 25% glycerol, 547 μ M CK-571.

X-ray data sets were collected at the Proxima 1 beamline at the Synchrotron SOLEIL at 100K and at wavelength of 0.97857 Å. The diffraction datasets were indexed and scaled with XDS³⁰. Molecular replacement solution was obtained with Phaser, CCP4 suite^{31,32} using the PDB entry 1BR1²⁶ as search model. The region of the converter, the Relay and the SH1 helix were excluded from the search model. These regions were subsequently built in electron density using the ARP/wARP program^{33,34}. The coordinate and geometry constraints files for the ligand were created with Sketcher of the CCP4 suite and Elbow of the Phenix suite^{35,36}. Model building and refinement were carried out with Coot³⁷ and Buster programs³⁸. In the final Ramachandran plot, 96.29%, 3.28% and 0.43% of residues were in the favored, allowed and outliers regions, respectively. Figures and movies were made using PyMol³⁹.

Note that crystals with CK-571 bound can be obtained in the presence of MgADP as well as other ATP analogs and the structure solved with ADP bound is essentially the same as that we report here with MgADP.BeFx bound.

Small Angle X-ray Scattering (SAXS) experiments

SAXS data were collected on the SWING beamline (synchrotron SOLEIL, France). Purified smooth muscle myosin S1 fragment was incubated with 2 mM MgADP for 30 minutes on ice. The protein was then incubated with either 5 mM CK-571 or 10% DMSO for 1h on ice, followed by the incubation with 2 mM vanadate or 2 mM BeFx for 30 minutes on ice when necessary. All samples were centrifuged at 20,000g for 10 min at 4°C prior to the analysis. 40 μ l of the protein at 3 mg/ml were injected between two air bubbles using the auto-sampler robot. 35 frames of 1.5s exposure were averaged and buffer scattering was subtracted from the sample data. The SM/CK-571 S1 model was built using the SM/CK-571 motor domain and the helix and ELC from previous smooth myosin structures (1BR1) using the converter position as a reference. The theoretical SAXS curve of this model was calculated with CRY SOL⁴⁰ and compared based on the quality of their fits against the different experimental curves.

Biochemical Assays:

ATPase Assays

Steady-state ATPase assays were performed at 22°C in PM12 buffer (12 mM K-PIPES, 2 mM MgCl₂, pH 6.8) containing 250 μ M ATP. Basal and actin-stimulated ATPase activities were measured using a spectrophotometric ATPase assay that couples ADP production to the oxidation of NADH using pyruvate kinase and lactate dehydrogenase². SMM S1 concentration was estimated by OD280 in 6M guanidine HCl using a molar absorption coefficient of 95793 M⁻¹ cm⁻¹ calculated based on the sequence of chicken MYH11 (1-843) and light chain MYL6. Specificity and intrinsic potency of CK-571 was determined using EDC/NHS-crosslinked Acto-S1 proteins (see above) as well as a highly sensitive spectrofluorometric ATPase assay that couples ADP production to the conversion of Amplex Red into resorufin using pyruvate kinase, pyruvate oxidase, and horseradish peroxidase while regen-

erating ATP. Hydrolysis rates were normalized using reactions containing an equivalent concentration of DMSO (activity=100%) and fit with a four parameter logistic curve (GraphPad Prism) without additional background subtraction or data manipulation.

Actin co-sedimentation assay

Myosin binding to actin was measured by depletion of soluble myosin from binding reactions using 3 μ M recombinant chicken Smooth Muscle Myosin MDE (1-819) and 6 μ M bovine cardiac actin in PM12 buffer. ATP and ADP were present at 1 mM where indicated, and hexokinase (10 U/ml) and glucose (2 mM) were added to nucleotide-free and ADP reactions to deplete residual ATP. Phalloidin (6 μ M) was included to stabilize actin filaments. Reactions were allowed to equilibrate at 22°C for 10 minutes prior to centrifugation (540k x g, 30 minutes), with ATP added just prior to centrifugation to minimize hydrolysis. Supernatants were analyzed by SDS-PAGE followed by staining with Coomassie brilliant blue.

Transient kinetics

Chemical hydrolysis of ATP was measured in PM12 buffer at 25°C by rapid mixing quench-flow (Biologic SFM/400, Bio-logic Inc.) under multiple turnover conditions and by manual quench in single turnover conditions (as shown in Fig. 1f). Native chicken gizzard SMM S1 (15 μ M) was preincubated with DMSO or CK-571 in DMSO (25 μ M) before rapid mixing with ATP (150 μ M), ageing, and quenching with 0.6M perchloric acid. ATP hydrolysis was monitored using malachite green to quantify total acid-labile phosphate⁴¹. The effect of CK-571 on ATP hydrolysis was further verified by measuring the burst size under single turnover conditions. Myosin (30 μ M) was preincubated with DMSO (2%) or CK-571 in DMSO (50 μ M), manually mixed 1:1 with ATP (10 μ M), aged for 5 seconds, and then quenched by addition of perchloric acid (0.3M final) prior to phosphate detection using malachite green.

Mant-ATP binding was measured in PM12 buffer at 25°C by rapid mixing stopped-flow (SF61DX2, TdK Scientific) (Supplementary Fig.2c). Mant-ATP fluorescence was monitored by excitation at 360nm while monitoring emission through a 400nm long pass filter. 2 μ M SMM S1 and 6 μ M F-actin were mixed to form the rigor state and 6 μ M CK571 or DMSO was also mixed prior to addition of Mant-ATP at different concentrations.

Isothermal titration calorimetry

Isothermal titration calorimetry experiments were carried out using a Micro-Cal Auto ITC HT microcalorimeter (Microcal Inc, now Malvern, Inc.) at 10°C. A solution of 125 μ M CK-571 in 12 mM PIPES (pH 6.8), 2 mM MgCl₂, 5 mM β -mercaptoethanol, and 3% DMSO (pH 6.8) was titrated into the sample cell, which contained 8 μ M chicken gizzard SMM S1 in the same buffer. SMM S1 concentration was estimated by OD280 in 6M guanidine HCl using a molar absorption coefficient of 95793 M⁻¹ cm⁻¹ calculated based on the sequence of chicken MYH11 (1-843) and light chain MYL6. Injections (10 μ L) were made every 300 seconds. To correct for the heats of dilution and slight buffer mismatches between the titrant and sample, the average heat signal from the last three injections at the end of the experiment (when binding was saturated) was subtracted from all values. Data collection and analysis was performed using the modified Origin software included with the instrument, using a single binding site model. Nucleotides and nucleotide analogs were present at 2 mM. To measure affinity in the absence of nucleotide, apyrase (Sigma A-6535) was included in the myosin sample at 17 μ g/ml.

Tissue and In Vivo Assays:

Animal care and welfare

Animals used in this study were maintained in accordance with the Guide for the Care and Use of Laboratory Animals of the Institute (National Research Council) and under the supervision of the Institutional Animal Care and Use Committee (IACUC) of Cytokinetics for rodent studies or LRR1 for canine studies.

Skinned Ring Contractility

Endothelium-denuded rat tail artery segments were cut into 3-mm helical rings, mounted on an isometric force transducer with a resting tension of 0.5 g, and incubated for 30 min at room temperature in normal HEPES-Tyrode buffer (135 mM NaCl, 6 mM KCl, 1.2 mM MgCl₂, 12 mM HEPES, 2.5

mM CaCl₂, 0.21 % glucose (w/v), pH 7.4). Tissues were skinned by incubation with skinning solution (30 mM TES, 50 mM KCl, 5 mM K₂EGTA, 5.1% sucrose (w/v), 0.5 mM DTE, 1% Triton X-100, pH 6.9) for 1 hour at room temperature. Tissues were preincubated in assay buffer (30 mM TES, 5.6 mM MgCl₂, 75 mM K-propionate, 3.8 mM ATP, 16 mM creatine phosphate, 15 U/ml creatine phosphokinase, 0.5 mM DTT, 4 mM K-EGTA and sufficient calcium to yield the desired free calcium concentrations, pH 6.9) containing DMSO or CK-571 in DMSO for 15 minutes prior to the addition of calcium. The force generated at the plateau of each calcium condition was recorded, and data were presented as a percent change from the baseline values⁴². Dose-response data were fit with a three-parameter equation (assumed Hill slope = 1).

Thiophosphorylation Assay

Triton-permeabilized endothelium-denuded rat tail artery preparations (see above) were prepared and mounted as above, then incubated in rigor solution containing ATP- γ -S (1 mM) for 10 min. Tissues were preincubated with CK-571 for 15 minutes prior to the addition of ATP. ATP-induced contraction was measured for 60 minutes and the relaxation was expressed as percentage of the maximum force.

Intact Tracheal Ring Contractility

Rat trachea were dissected and placed into cold Krebs-Henseleit buffer (117.5 mM NaCl, 4.7 mM KCl, 1.2 mM KH₂PO₄, 1.18 mM MgSO₄, 2.5 mM CaCl₂, 25 mM NaHCO₃, 11 mM glucose) equilibrated with 95% O₂/5% CO₂. Trachea were cut into 2 mm rings and mounted in a tissue bath (Radnoti LLC, Monrovia, CA) containing Krebs-Henseleit buffer equilibrated with 95% O₂/5% CO₂ at 37°C. Rings were stretched to a baseline isometric tension of 2g, and then induced to contract with a submaximal dose of methacholine (3 μ M). Rings were relaxed by treatment with ascending doses of CK-571 in DMSO. Force values were normalized to the initial methacholine-induced value for each ring. Dose-response data were fit with a four-parameter equation.

Bronchoconstriction Measurements in Naïve Dogs

Naïve beagles (10.5-14kg, 2.6-3 years of age) were used for this study. The response of naïve beagles (n=8, 10.5-14kg, 2.6-3 years of age) to increasing ½ log doses of inhaled methacholine (MCh, 0.3, 1, 3, 5, 10, 30, 50, 100, etc. mg/ml), was characterized to determine the concentration that induced a 200 -250% increase in pulmonary resistance. A subset of four animals (two male, two female) were selected for further study. An abbreviated MCh dose response (up to 3 doses) was performed to confirm the dose of MCh that induces a 200 – 250% increase in pulmonary resistance. Fifteen minutes later a single dose of MCh was again given to reconfirm the response. The response to this challenge was used to compare all subsequent MCh challenges following test article treatment. Treatment with inhaled CK-571 (100 μ g/kg via insufflator) or albuterol (10 μ g/kg via nebulizer) was given 15 minutes following the single MCh challenge. MCh challenge was repeated at 5, 20, 40, 60, 90, 120, 180 and 240 minutes post-test article treatment. The repeated MCh challenges were aimed at evaluating the duration of action of the test article. The dogs were rested at least ~ 7 – 14 days in between each dose to allow time for washout of the previous dose.

Acknowledgments

We thank Pierre Legrand and Andrew Thompson as well as beamline scientists of PX1 (SOLEIL synchrotron) for excellent support during data collection. A.H. was supported by grants from FRM, ANR, AFM and ARC. The AH team is part of Labex CeTisPhyBio:11-LBX-0038, which is part of the IDEX PSL (ANR-10-IDEX-0001-02 PSL). **ACCESSION CODES** Coordinates and structure factors have been deposited in the Protein Data Bank under accession code **5T45**. **Author contributions** A.H., F.I.M. and J.H. designed research; S.S., V.J.P-H., V.R., E.A.S. and A.H. were involved in crystallization and structure determination; S.C., G.C., X.Q, P.L., B.M. performed *in vitro* functional assays; K.R., C.R., E.B. carried out *in vivo* assays; A.H. and J.H. analyzed the data; A.H. wrote the manuscript with the help of the other authors.

1. Sweeney, H.L. & Houdusse, A. (2010) Structural and functional insights into the Myosin motor mechanism. *Annu Rev Biophys.* **39**:539-57.
2. Malik, F.I. *et al.*, (2011) Cardiac myosin activation: a potential therapeutic approach for systolic heart failure. *Science* **331**:1439-43.
3. Bond, L.M., Tumbarello, D.A., Kendrick-Jones, J. & Buss F. (2013) Small-molecule inhibitors of myosin proteins. *Future Med. Chem.* **5**:41-52.
4. Green EM, *et al.*, Seidman CE. (2016) A small-molecule inhibitor of sarcomere contractility suppresses hypertrophic cardiomyopathy in mice. *Science.* **351**:617-21.
5. Berair, R., Hollins, F. & Brightling, C. (2013) Airway smooth muscle hypercontractility in asthma. *J. Allergy* **2013**:185971.
6. Dowell, M.L., Lavoie, T.L., Solway, J. & Krishnan, R. (2014) Airway smooth muscle: a potential target for asthma therapy. *Curr Opin Pulm Med.* **20**:66-72.
7. Wedzicha, J.A., Decramer, M. & Seemungal, T.A. (2012) The role of bronchodilator treatment in the prevention of exacerbations of COPD. *Eur Respir J.* **40**:1545-54.
8. Winkelmann, D.A., Forgacs, E., Miller M.T. & Stock, A.M. (2015) Structural basis for drug-induced allosteric changes to human β -cardiac myosin motor activity. *Nat. Commun.* **6**:7974.
9. Liu, Y., White, H.D., Belknap, B., Winkelmann, D.A. & Forgacs, E. (2015) *Omeceamtiv Mecarbil* modulates the kinetic and motile properties of porcine β -cardiac myosin. *Biochemistry.* **54**:1963-75.

10. Allingham, J.S., Smith, R. & Rayment, I. (2005) The structural basis of blebbistatin inhibition and specificity for myosin II. *Nat Struct Mol Biol.* **12**:378-9.
11. Fedorov, R. *et al.*, (2009) The mechanism of pentabromopseudilin inhibition of myosin motor activity. *Nat Struct Mol Biol.* **16**:80-8.
12. Limouze, J., Straight, A.F., Mitchison, T. & Sellers, J.R. (2004) Specificity of blebbistatin, an inhibitor of myosin II. *J Muscle Res Cell Motil.* **25**:337-41.
13. Koppole, S., Smith, J.C. & Fischer, S. (2007) The structural coupling between ATPase activation and recovery stroke in the myosin II motor. *Structure* **15**:825-37.
14. Elber, R. & West, A. (2010) Atomically detailed simulation of the recovery stroke in myosin by Milestoning. *Proc Natl Acad Sci USA.* **107**:5001-5.
15. Yu, H., Ma, L., Yang, Y. & Cui, Q. (2007) Mechanochemical coupling in the myosin motor domain. I. Insights from equilibrium active-site simulations. *PLoS Comput Biol.* **3**:e21.
16. Daily, M.D., Yu, H., Phillips, G.N. Jr & Cui, Q. (2013) Allosteric activation transitions in enzymes and biomolecular motors: insights from atomistic and coarse-grained simulations. *Top Curr Chem.* **337**:139-64.
17. Nesmelov, Y.E. *et al.* (2011) Structural kinetics of myosin by transient time-resolved FRET. *Proc Natl Acad Sci USA.* **108**:1891-6.
18. Houdusse, A., Kalabokis, V.N., Himmel, D., Szent-Györgyi, A.G. & Cohen, C. (1999) Atomic structure of scallop myosin subfragment S1 complexed with MgADP: a novel conformation

953 of the myosin head. *Cell*. **97**:459-70.
 954 19. Himmel, D. *et al.* (2002) Crystallographic findings on the internally uncoupled and near-rigor
 955 states of myosin: further insights into the mechanics of the motor. *Proc Natl Acad Sci USA*.
 956 **99**:12645-50.
 957 20. Sweeney H.L., Houdusse, A. (2010) Myosin VI rewrites the rules for myosin motors. *Cell*.
 958 **141**:573-82.
 959 21. Dunn T.A. *et al.* (2006) A novel role of myosin VI in human prostate cancer. *Am J Pathol*.
 960 **169**:1843-54.
 961 22. Yoshida H. *et al.* (2004) Lessons from border cell migration in the Drosophila ovary: A role
 962 for myosin VI in dissemination of human ovarian cancer. *Proc Natl Acad Sci USA*. **101**:8144-9.
 963 23. Knudsen, B. (2006) Migrating with myosin VI. *Am J Pathol*. **169**:1523-6.
 964 24. Arjonen, A., Kaukonen, R. & Ivaska, J. (2011) Filopodia and adhesion in cancer cell motility.
 965 *Cell Adh Migr*. **5**:421-30.
 966 25. Sellers, J.R., Pato, M.D. & Adelstein, R.S. (1981) Reversible phosphorylation of smooth
 967 muscle myosin, heavy meromyosin, and platelet myosin. *J. Biol. Chem.* **256**:13137-42.
 968 26. Dominguez, R., Freyzon, Y., Trybus, K.M. & Cohen, C. (1998) Crystal structure of a
 969 vertebrate smooth muscle myosin motor domain and its complex with the essential light
 970 chain: visualization of the pre-power stroke state. *Cell* **94**:559-71.
 971 27. Margossian, S.S. & Lowey, S. (1982) Preparation of myosin and its subfragments from rabbit
 972 skeletal muscle. *Methods Enzymol.* **85**:55.
 973 28. Mornet, D., Bertrand, R., Pantel, P., Audemard, E. & Kassab, R. (1981) Structure of the
 974 actin-myosin interface. *Nature* **292**:301-6.
 975 29. Bonafe, N. & Chaussepied, P. (1995) A single myosin head can be cross-linked to the N
 976 termini of two adjacent actin monomers. *Biophys. J.* **68**:35S.
 977 30. Kabsch, W. XDS. (2010) *Acta Cryst.* **D66**:125-32.
 978 31. Collaborative Computational project, Number 4, The CCP4 Suite: Programs for Protein
 979 Crystallography. (1994) *Acta Cryst.* **D50**:760-3.

32. McCoy, A.J. Phaser crystallographic software. (2007) *J. Appl. Cryst.* **40**:658-74.
 33. Langer, G., Cohen, S.X., Lamzin, V.S. & Perrakis, A. (2008) Automated macromolecular
 model building for X-ray crystallography using ARP/wARP version 7. *Nat. Protoc.* **3**:1171-9.
 34. Winn, M. *et al.* (2011) Overview of the CCP4 suite and current developments. *Acta Cryst.*
D67:235-42.
 35. Adams, P. *et al.* (2011) The Phenix software for automated determination of macromolecular
 structures. *Methods* **55**:94-106.
 36. Moriarty, N., Grosse-Kunstleve, R. & Adams, P. (2009) Electronic Ligand Builder and
 Optimization Workbench (eLBOW): a tool for ligand coordinate and restraint generation.
Acta Cryst. **D65**:1074-80.
 37. Emsley, P., Lohkamp, B., Scott, W.G. & Cowtan, K. (2010) Features and development of
 Coot. *Acta Cryst.* **D66**:486-501.
 38. Bricogne, G. *et al.* (2011) BUSTER version 2.10.1 Cambridge, United Kingdom: Global
 Phasing Ltd..
 39. PyMOL Molecular Graphics System, Version 1.5.0.4 Schrödinger, LLC.
 40. Svergun, D.I., Barberato, C. & Koch, M.H.J. (1995) CRY SOL - a Program to Evaluate X-ray
 Solution Scattering of Biological Macromolecules from Atomic Coordinates. *J. Appl. Cryst.*
28:768-73.
 41. Baykov, A.A., Evtushenko, O.A. & Avaeva, S.M. (1988) A malachite green procedure for
 ortho-phosphate determination and its use in alkaline phosphatase-based enzyme immunoas-
 say. *Anal. Biochem.* **171**:266-70.
 42. Wilson, D.P., Sutherland, C. & Walsh, M.P. (2002) Ca²⁺ activation of smooth muscle
 contraction: evidence for the involvement of calmodulin that is bound to the triton insoluble
 fraction even in the absence of Ca²⁺. *J. Biol. Chem.* **277**:2186-92.

1021
1022
1023
1024
1025
1026
1027
1028
1029
1030
1031
1032
1033
1034
1035
1036
1037
1038
1039
1040
1041
1042
1043
1044
1045
1046
1047
1048
1049
1050
1051
1052
1053
1054
1055
1056
1057
1058
1059
1060
1061
1062
1063
1064
1065
1066
1067
1068
1069
1070
1071
1072
1073
1074
1075
1076
1077
1078
1079
1080
1081
1082
1083
1084
1085
1086
1087
1088

Submission PDF

Supplementary Material for

Highly selective inhibition of myosin motors – the basis of potential therapeutic application

S. Sirigu^{1#}, J. Hartman^{3#}, V.J. Planelles-Herrero^{1,2#}, V. Ropars¹, S. Clancy³, G. Chuang³, X. Qian³, P. Lu³, E. Barrett⁴, K. Rudolph⁴, C. Royer⁴, B. Morgan³, E.A. Stura⁵, F.I. Malik³, A. Houdusse^{1*}

#co-first authors

¹ Structural Motility, Institut Curie, PSL Research University, CNRS, UMR 144, F-75005, Paris, France.

² Sorbonne Universités, UPMC Univ Paris06, Sorbonne Universités, IFD, 4 Place Jussieu, 75252 PARIS cedex 05

³ Preclinical Research and Development, Cytokinetics, Inc., South San Francisco, CA 94080, USA

⁴ Lovelace Respiratory Research Institute, 2425 Ridgecrest Dr. SE, Albuquerque, NM 87108-5127, USA

⁵ CEA, DSV, iBiTec-S, Service d'Ingénierie Moléculaire des Protéines, 91191 Gif-sur-Yvette, France.

*Corresponding author. E-mail: Anne.Houdusse@curie.fr

This PDF file supplies:

Supplementary Figures 1 to 5
Supplementary Tables 1 and 2
Legends for Supplementary Movies 1 to 4
References (For Supplementary)

Other Supplementary Material for this manuscript includes Movies S1-S4

Supplementary Figures

a

```

Hs-SMM2      MAQKGQ-----LSDDEKFLVDKNFINS-----PVAQADWAARLWVWPS 40
Hs-NMM2a     MAQCA-----ADKYLVDKNFINN-----PVAQADWAARLWVWPS 36
Hs-NMM2b     MAQRFG-----LEDPERYLFVDAVIYN-----PVAQADWAARLWVWPS 40
Hs-NMM2c     MAAVTMSVPGKAPRPGPVLEAAQPLFETFRGPSAGGGGSGSTPQVWLTARRLWVWPS 60

Hs-SMM2      EKQGFEEASIKKEEGDEVVVELVENGKVKVVKDDIQKMNPPKFSKVEDMAELTCLNEAS 100
Hs-NMM2a     EKSGFEFASIKKEVGEELVELVENGKVKVVKDDIQKMNPPKFSKVEDMAELTCLNEAS 96
Hs-NMM2b     ERHGFEEASIKKEERGDEVVELVENGKVKVVKDDIQKMNPPKFSKVEDMAELTCLNEAS 100
Hs-NMM2c     ELHGFEEALRDEGEELEVELLESGRRLRPRDQIQKMNPPKFSKVEDMAELTCLNEAS 120

Hs-SMM2      VLHNLRYRYSGLIYTYSGLCVVPNPYKLPYSEIVEMYGKRRHEMPPHIYAITDT 160
Hs-NMM2a     VLHNLRYRYSGLIYTYSGLCVVPNPYKLPYSEIVEMYGKRRHEMPPHIYAITDT 156
Hs-NMM2b     VLHNLRYRYSGLIYTYSGLCVVPNPYKLPYSEIVEMYGKRRHEMPPHIYAITDT 160
Hs-NMM2c     VLHNLRYRYSGLIYTYSGLCVVPNPYKLPYSEIVEMYGKRRHEMPPHIYAITDT 180

Hs-SMM2      AYRSMQLDREDQSLILCTGSEAGKTENTKKVIQYLAHVASSHKKKDTSITGELKQLLQ 220
Hs-NMM2a     AYRSMQLDREDQSLILCTGSEAGKTENTKKVIQYLAHVASSHKKKDTSITGELKQLLQ 213
Hs-NMM2b     AYRSMQLDREDQSLILCTGSEAGKTENTKKVIQYLAHVASSHKKKDTSITGELKQLLQ 220
Hs-NMM2c     AYRSMQLDREDQSLILCTGSEAGKTENTKKVIQYLAHVASSHKKKDTSITGELKQLLQ 240

Hs-SMM2      ANP ILEAFGNAKTVKNDSSRFGKFIKINFDVNGYIVGANIETYLLEKSRAIRQADERT 280
Hs-NMM2a     ANP ILEAFGNAKTVKNDSSRFGKFIKINFDVNGYIVGANIETYLLEKSRAIRQADERT 273
Hs-NMM2b     ANP ILEAFGNAKTVKNDSSRFGKFIKINFDVNGYIVGANIETYLLEKSRAIRQADERT 280
Hs-NMM2c     ANP ILEAFGNAKTVKNDSSRFGKFIKINFDVAGYIVGANIETYLLEKSRAIRQADERT 300

Hs-SMM2      FHIFYMIAGAKEKMRSDLLLEGFNNTFLSNGFVPIPAQDDMFQETVEAMAIMGFSE 340
Hs-NMM2a     FHIFYLLSGAGELKSDLLLEGFNNTFLSNGHVTIPGQDKDMFQETVEAMAIMGFSE 333
Hs-NMM2b     FHIFYLLSGAGELKSDLLLEGFNNTFLSNGYIPIPGQDKDMFQETVEAMAIMGFSE 340
Hs-NMM2c     FHIFYLLSGAGELKSDLLLEGFNNTFLSNGYIPIPGQDKDMFQETVEAMAIMGFSE 359

Hs-SMM2      EEQLSILKVVSVLQGNIVFKKERTDQASMPDNTAAQKCHLMGINVDFTRSLTFR 400
Hs-NMM2a     EEQMGILRIVSGVLQGNIVFKKERTDQASMPDNTAAQKCHLMGINVDFTRSLTFR 393
Hs-NMM2b     EEQLSILKVVSVLQGNIVFKKERTDQASMPDNTAAQKCHLMGINVDFTRSLTFR 400
Hs-NMM2c     EETISLIRVSAVLQGNIVFKKERTDQASMPDNTAAQKCHLMGINVDFTRSLTFR 419

Hs-SMM2      IKVGRDVVQKAQTKQADFAVEALAKATYERLFRWILTRVINKALDKTRQGASFLGILD 460
Hs-NMM2a     IKVGRDVVQKAQTKQADFAVEALAKATYERLFRWILTRVINKALDKTRQGASFLGILD 453
Hs-NMM2b     IKVGRDVVQKAQTKQADFAVEALAKATYERLFRWILTRVINKALDKTRQGASFLGILD 460
Hs-NMM2c     IKVGRDVVQKAQTKQADFAVEALAKATYERLFRWILTRVINKALDKTRQGASFLGILD 479

Hs-SMM2      AGFEIFEVNSFEQLCINYNTEKIQQLFNHTMILEQEEYQREGIEWNFIDFGLDLPQCIE 520
Hs-NMM2a     AGFEIFEVNSFEQLCINYNTEKIQQLFNHTMILEQEEYQREGIEWNFIDFGLDLPQCIE 513
Hs-NMM2b     AGFEIFEVNSFEQLCINYNTEKIQQLFNHTMILEQEEYQREGIEWNFIDFGLDLPQCIE 520
Hs-NMM2c     AGFEIFEVNSFEQLCINYNTEKIQQLFNHTMILEQEEYQREGIEWNFIDFGLDLPQCIE 539

Hs-SMM2      LIERPNNPGLLALLDEECWFPKATDKSFVEKLCTEQGSHPKFKPKLKKKTEFSIIHY 580
Hs-NMM2a     LIERPAGPGLLALLDEECWFPKATDKSFVEKVMQEGQTHPKFKPKLKKKADFCIIHY 573
Hs-NMM2b     LIERPANNPGLLALLDEECWFPKATDKSFVEKLVQEGSSHFKPKPKLKKKADFCIIHY 580
Hs-NMM2c     LIERPANNPGLLALLDEECWFPKATDKSFVEKVAQEGGHPKFKPKLKKKADFCIIHY 599

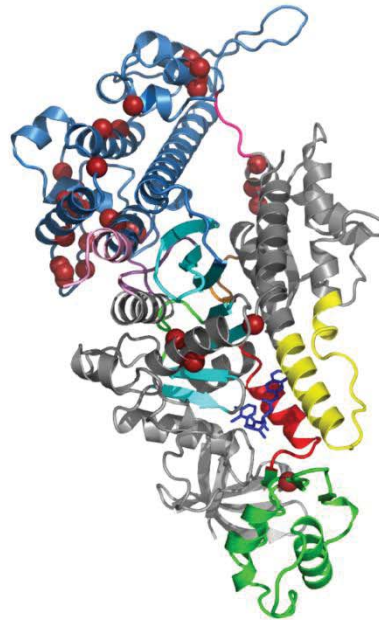
Hs-SMM2      AGKVDYNASAWLKNMDFLNDNVAALLHSSDKEFVADLWVKDVRIVGLDQAKMTESSLP 640
Hs-NMM2a     AGKVDYKADENLKNMDFLNDNVAALLHSSDKEFVADLWVKDVRIVGLDQAKMTESSLP 633
Hs-NMM2b     AGKVDYKADENLKNMDFLNDNVAALLHSSDKEFVADLWVKDVRIVGLDQAKMTESSLP 640
Hs-NMM2c     AGKVDYKADENLKNMDFLNDNVAALLHSSDKEFVADLWVKDVRIVGLDQAKMTESSLP 657

Hs-SMM2      SASKTKKGMFRVTGQLYKESLTKLMTLRNTTPEVRCIIPNHEKRSKGLDAPLVLEQLR 700
Hs-NMM2a     GAFKTRKGMFRVTGQLYKESLTKLMTLRNTTPEVRCIIPNHEKRSKGLDAPLVLEQLR 693
Hs-NMM2b     SASKTKKGMFRVTGQLYKESLTKLMTLRNTTPEVRCIIPNHEKRSKGLDAPLVLEQLR 700
Hs-NMM2c     FGGRPRKGMFRVTGQLYKESLTKLMTLRNTTPEVRCIIPNHEKRSKGLDAPLVLEQLR 717

Hs-SMM2      CNGVLEGIRICRQGFNRIYVQEFRQRYEILLAANAIPKGFMDGKQACILMKALELDPNL 760
Hs-NMM2a     CNGVLEGIRICRQGFNRIYVQEFRQRYEILLTNSIPKGFMDGKQACILMKALELDPNL 753
Hs-NMM2b     CNGVLEGIRICRQGFNRIYVQEFRQRYEILLTNSIPKGFMDGKQACERMLKALELDPNL 760
Hs-NMM2c     CNGVLEGIRICRQGFNRIYVQEFRQRYEILLTNSIPKGFMDGKQACERMLKALELDPNL 777

Hs-SMM2      YRIGQSKIFFRGTGLAHLEERDLKIDTVIMAFQAMCRGYLARKAFARQQQLTAMKVIQ 820
Hs-NMM2a     YRIGQSKVFFRGTGLAHLEERDLKIDTVIMAFQACCRGYLARKAFARQQQLTAMKVLQ 813
Hs-NMM2b     YRIGQSKIFFRGTGLAHLEERDLKIDTVIMAFQAVCRGYLARKAFARQQQLTAMKVIQ 820
Hs-NMM2c     YRIGQSKIFFRGTGLAHLEERDLKIDTVIMAFQAVCRGYLARKAFARQQQLTAMKVIQ 837
    
```

b

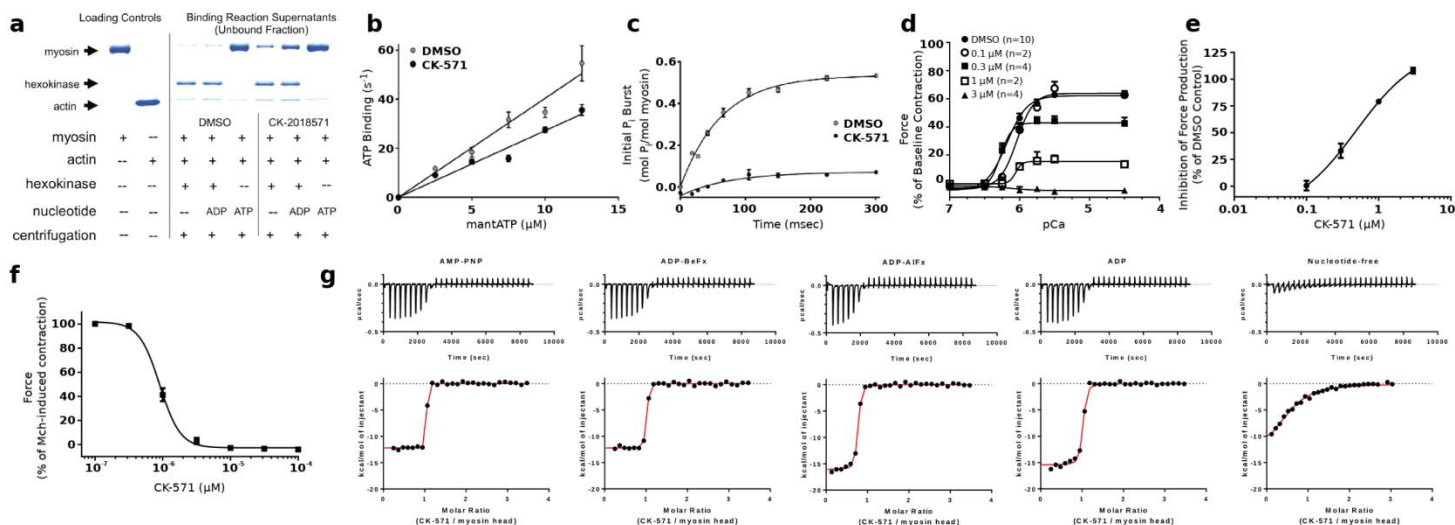


c

Nterm		***	*	*
Hs-Smooth-MyoII		DMAE	LTCLN	EASVLH
Hs-Cardiac-MyoII		DMAM	LTFLH	EPAVLY
Hs-Skeletal-MyoII		DMAM	MTHLH	EPAVLY
Transducer			****	
Hs-Smooth-MyoII			GLIYTYSGLCFVTV	
Hs-Cardiac-MyoII			WMIYTYSGLCFVTV	
Hs-Skeletal-MyoII			WMIYTYSGLCFVTV	
Relay		**	*	*
Hs-Smooth-MyoII		QQLFNHTM	FILEQEEYQREG	IEWNFIDFGLD
Hs-Cardiac-MyoII		QQFFNHHM	FVLEQEEYKKEG	IEWTFIDFGMD
Hs-Skeletal-MyoII		QQFFNHHM	FVLEQEEYKKEG	IEWTFIDFGMD
L50		*		
Hs-Smooth-MyoII		SIIHYA	GKVDYN	
Hs-Cardiac-MyoII		SLIHYA	GIVDYN	
Hs-Skeletal-MyoII		ALIIHYA	GVVDYN	
SH1 helix		**	****	**
Hs-Smooth-MyoII		LRCN	GVLEGIRICRQG	FPNRIV
Hs-Cardiac-MyoII		LRCN	GVLEGIRICRKG	FPNRIL
Hs-Skeletal-MyoII		LRCN	GVLEGIRICRKG	FPSRIL

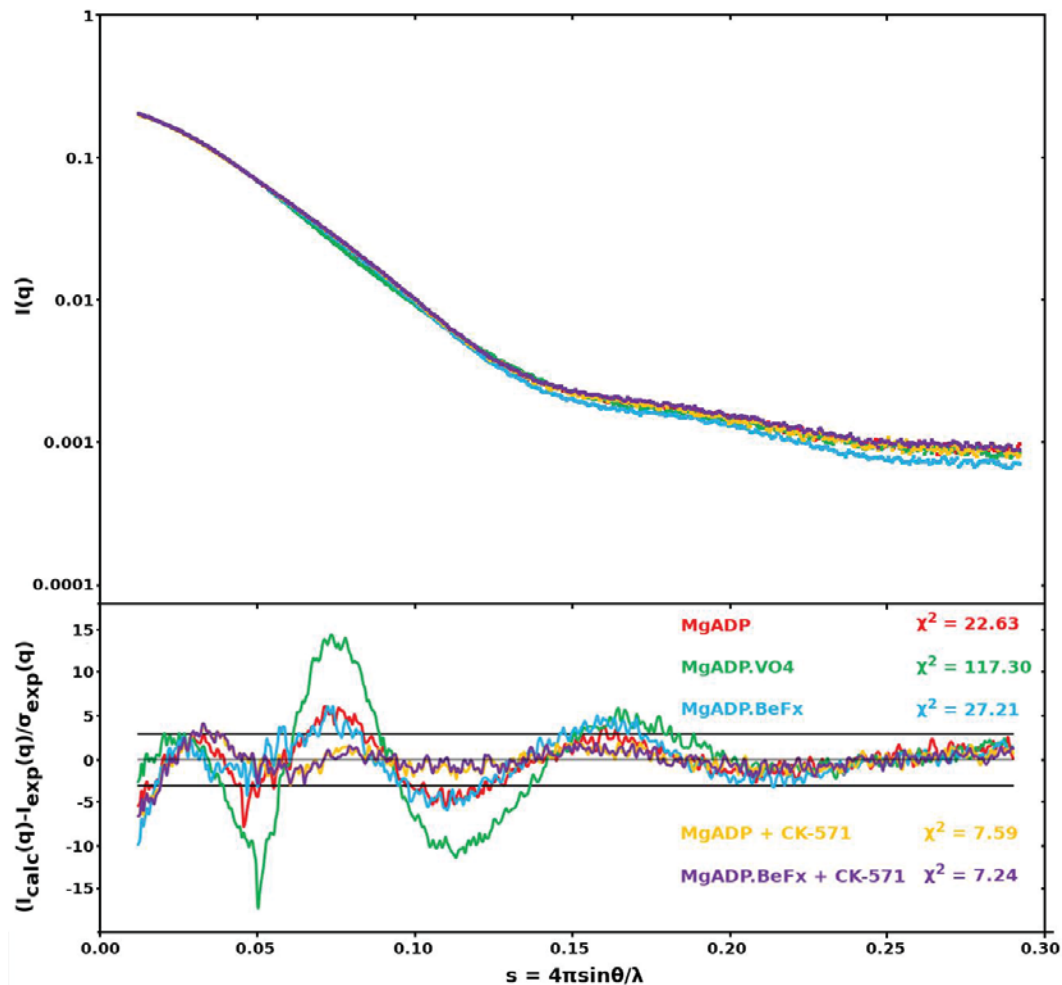
Supplementary Figure 1. (a) Sequence alignment of the heavy chain of Human Smooth Muscle Myosin II (Hs-SMM2) and Non Muscle Myosin II isoform a, b, c (Hs-NMM2 a, b, c). Residues that are not conserved are shown in yellow; similar residues that are not conserved are green. Residues involved in the binding of CK-571 are labelled with a star highlighted cyan: none of these residues are different in sequence between smooth and non-muscle myosins. Human SMM2 and NMM2a, NMM2b, NMM2c share respectively 83%, 84%, 75% sequence identity and 91%, 91%, 88% sequence similarity in their motor domain. Note the main sequence differences noted with the symbol # and the sequence for Loop1 and Switch II indicated respectively in red and blue. In between these two elements, the sequence corresponds to residues of the U50 subdomain. The kinetics of the allosteric

rearrangements occurring in the recovery stroke depends on the full sequence of the myosin motor and determines the specific kinetic rates of ATP hydrolysis. In transient kinetic studies, the rate that measures both the recovery stroke isomerisation and hydrolysis ($k_{+3}+k_{-3}$) is faster for SMM2² ($k_{+3}+k_{-3} = 50 \text{ s}^{-1}$) compared to NMM2A³ ($k_{+3}+k_{-3} = 14 \text{ s}^{-1}$) and NMM2B⁴ ($k_{+3}+k_{-3} = 16.7 \text{ s}^{-1}$). Differences in the U50 subdomain or the loop1 sequence are the most likely candidates to influence the overall dynamics in this transition, in particular by controlling the rearrangements necessary in the transducer for this transition (Fig. S4C). Thus, specificity in the inhibition depends on the dynamics of this reversible transition that is modulated by residues that are far from the drug binding site. **(b)** Residues that are not conserved between Hs SMM2 and NMM2 and are likely candidates to modulate the recovery stroke are shown with brown spheres on the SM/CK-571 structure (see also Movie S2). **(c)** Sequence alignment of Human Skeletal, Cardiac and Smooth Myosin II. Residues involved in CK-571 binding are labelled with a star. Note that they are all identical in these different myosins.

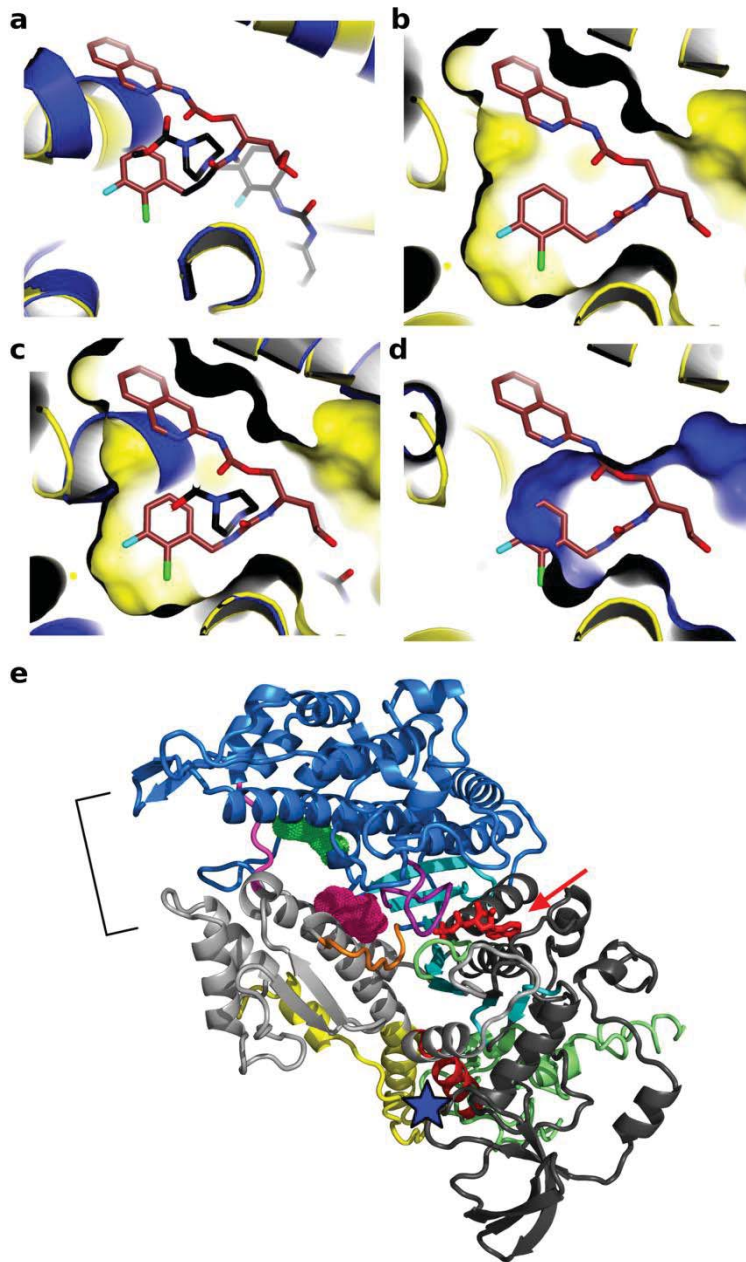


Supplementary Figure 2. Characterization of the mechanism of CK-571 *in vitro*.

(a) CK-571 (50 μM) inhibits SMM in a weak actin-binding state, as indicated by presence of equal or greater quantities of SMM in the supernatants from actin-binding reactions containing CK-571 as compared with DMSO. This is most obvious for the motor bound with ADP, which allows strong binding to F-actin in the absence of drug but not in its presence. In the presence of ATP and saturating CK-571, essentially all SMM is dissociated. The drug binding site is not as easily reachable when no nucleotide is bound and to a lesser extent when ADP is bound. This limits the degree to which drug binding prevents actin binding in these states. **(b)** CK-571 has minimal effects on the rate of ATP binding to nucleotide-free actin-bound SMM (CK-571=2.8 $\mu M^{-1} \cdot s^{-1}$, DMSO=4.0 $\mu M^{-1} \cdot s^{-1}$) as measured using mantATP (plotted is mean \pm SEM for 5 replicates). **(c)** CK-571 slows the rate of ATP hydrolysis (CK-571=4 s^{-1} , DMSO=16 s^{-1}), and reduces the size of the phosphate burst (CK-571=0.1, DMSO=0.53) as measured by chemical quench flow using a 10-fold excess of ATP (plotted is mean \pm SD for 4 replicates). **(d)** CK-571 inhibits Ca^{2+} -dependent force production in skinned rat caudal artery rings (plotted is mean \pm SEM). **(e)** Dose-response of CK-571 inhibition in skinned rat caudal artery rings at pCa 4.5 (plotted is mean \pm SEM, EC50 = 0.49 μM). **(f)** CK-571 dose-dependently relaxes intact rat tracheal rings precontracted with 3 μM methacholine. (plotted is mean \pm SEM, n=12, EC50 = 0.90 μM , Hill slope = 2.9). **(g)** Isothermal titration calorimetry (ITC) experiments in the presence of AMP-PNP, ADP-BeFx, ADP-AIFx, ADP and in the absence of nucleotide.



Supplementary Figure 3. Small-angle X-ray Scattering (SAXS) analysis of the SM/CK-571 structure. The SMM S1 fragment was analyzed by SAXS in several nucleotide-bound conditions (MgADP, MgADP.VO4, MgADP.BeFx, MgADP+CK-571 and MgADP.BeFx +CK-571) that allow population of different states of the motor cycle. The scattering pattern of the SMM S1 fragment that correspond to the SM/CK-571 crystal structure we have obtained was calculated and fit against the experimental scattering curves. **Upper graph:** experimental scattering intensities. **Lower graph:** reduced residuals of the least-squares fits on a linear scale. Two horizontal lines define the $\pm 3\sigma$ range. The χ^2 value reflects the discrepancy between theoretical and experimental curves. Note how similar are the MgADP+CK-571 and MgADP.BeFx+CK-571 curves (purple, yellow), and how they differ from that of MgADP.VO4 (green).



Supplementary Figure 4. Modulators of myosin activity differently influence the recovery stroke and its ability to produce force. Representation of the CK-571 (brown) and *omecamtiv mecarbil* (4PAO, black) binding pockets. The binding site for CK-571 (orange) is distinct from that of myosin activator *omecamtiv mecarbil* (blue). Note that there is poor superimposition between the structural elements that surround the ligand binding pockets (a) and none of the rings of CK-571 fit in the pocket in which *omecamtiv mecarbil* binds (b-d). Note in particular how the binding surface of CK-571 (b) differs from that of *omecamtiv mecarbil* (d). (e) Representation of the *Dictyostelium discoideum* myosin II structure (PDB 2JHR, 1YV3) in a PPS state showing that blebbistatin (pink) and pentabromopseudilin (green) occupies surface pockets of the PPS state that are close to the ATP (red arrow) or the actin binding site (bracket) respectively. These sites are distant from the CK-571 site (blue star). Note that no pocket is available for CK-571 binding in the PPS state.

Nterm

	***	*	*	
Hs-Smooth MyoII	DMAE	LTCLN	EASVLH	88-102
Hs-Myo VI	DNCS	LMYLN	EATLLH	61-75
Hs-Myo VIIa	DMIR	LGDLN	EAGILR	69-83
Hs-Myo XVIIIa	DIAS	LVYLN	ESSVLH	409-423
Hs-Myo Va	DLTA	LSYLH	EPAVLH	73-87
Hs-Myo X	DMAS	LTELH	GGSIMY	67-81

Transducer

Hs-Smooth MyoII	GLIYTYSGLFCVV	112-124
Hs-Myo VI	DRIYTYVANILIA	84-96
Hs-Myo VIIa	HLIYTYTGSILVA	92-104
Hs-Myo XVIIIa	SLLHTYAGPSLLV	432-444
Hs-Myo Va	KLIYTYCGIVLVA	97-109
Hs-Myo X	NQIYTYIGSILAS	90-102

Relay

	**	*	*		*
Hs-Smooth MyoII	QQLFNHTM	FILEQEEYQREG	IEWNFIDFGLD		491-521
Hs-Myo VI	QOFFNERI	LKEEQELYQKEG	LGVNEVH	YVD	481-510
Hs-Myo VIIa	QOFFVRHV	FKLEQEEYDLES	IDWLHIE	FTD	462-491
Hs-Myo XVIIIa	QRLFHERT	FVQELERYKEEN	IELAFDDLEPP		820-850
Hs-Myo Va	QQQFNMHV	FKLEQEEYMKEQ	IPWTLID	FYD	462-491
Hs-Myo X	QEYFNKHI	FSLEQLEYSREG	LVWEDID	WID	459-489

L50

	*		
Hs-Smooth MyoII	SIIHYA	GKVDY	583-593
Hs-Myo VI	IIRHFA	GAVCY	578-588
Hs-Myo VIIa	GINHFA	GIVYY	550-560
Hs-Myo XVIIIa	GHSHGT	NWVEY	930-940
Hs-Myo Va	IIQHFA	DKVEY	549-559
Hs-Myo X	GVKHYA	GEVQY	545-555

SH1 helix

	**	***	**		* *
Hs-Smooth MyoII	LRCN	GVLEGIRICRQG	FPNRIV		706-727
Hs-Myo VI	LQCS	GMVSVLDLMQGG	YPSRAS		689-710
Hs-Myo VIIa	LRYS	GMMETIRIRRAG	YPIRYS		656-678
Hs-Myo XVIIIa	LRGS	RLLDAMRMYRQG	YPDH MV		1096-1118
Hs-Myo Va	LRAC	GVLETIRISAAG	FPSRWT		680-702
Hs-Myo X	LRYS	GMLETVRIRKAG	YAVRRP		657-678

Supplementary Figure 5. Sequence alignment of Hs-Smooth Myosin II (Hs-SMM) and different Human Myosins.

Out of 24 residues that directly interact with CK-571, 10 are not conserved in HsMyoVI, 10 are not conserved in MyoXVIIIa, 7 are not conserved in MyoVIIa, 5 are not conserved in MyoVa, and 7 are not conserved in MyoX. Residues involved in CK-571 binding are labelled with a star. Residues that are similar but not identical are in blue, residues that are not conserved are in yellow.

Supplementary Table 1: Data Collection and Refinements statistics

SM/CK-571	
Data collection	
Space group	P2 ₁ 2 ₁ 2
Cell dimensions	
<i>a</i> , <i>b</i> , <i>c</i> (Å)	72.94, 202.17, 67.02
α , β , γ (°)	90.0, 90.0, 90.0
Resolution (Å)	50.00-2.65 (2.74-2.65)*
No. Reflections	
Total	202,529
Unique	29,002
Completeness (%)	99.0 (93.8)
Redundancy	6.98 (6.95)
<i>R</i> _{sym}	10.2 (76.2)
<i>I</i> / σ	14.23 (2.17)
Refinement	
Resolution (Å)	44.35-2.80 (2.91-2.80)
<i>R</i> _{work} / <i>R</i> _{free} (%)	21.89/27.11 (29.56/37.05)
R.m.s. deviations	
Bond lengths (Å)	0.010
Bond angles (°)	1.18
Number of atoms	
Non-hydrogen, protein	5,800
Drug	35
Water	84
ADP.BeFx	31
PDB CODE	5T45

*Values in parentheses are for highest-resolution shell. The structure was solved by molecular replacement with data from a single crystal.

Supplementary Table 2: Myosin II structures used for analysis and comparison

Post-rigor state, PR – prior to the Recovery Stroke

pdb:	3I5F	Squid skeletal muscle myosin II in post-rigor
	1SR6	Argopecten skeletal muscle myosin II in post-rigor
	2OTG	Placopecten skeletal muscle myosin II in post-rigor
	2MYS	Chicken skeletal muscle myosin II in post-rigor
	4DB1	Human beta cardiac muscle myosin II in post-rigor
	4P7H	Human beta cardiac muscle myosin II in post-rigor

Pre-powerstroke state, PPS – after the Recovery Stroke

pdb:	1QVI	Argopecten skeletal muscle myosin II in pre-powerstroke state
	1BR1	Chicken smooth muscle myosin II in pre-powerstroke state
	2YCU	Human non muscle myosin IIC in pre-powerstroke state

Other Supplementary Material for this manuscript includes Movies S1-S4.

Legends for Movies:

Movie S1. Structure of the Smooth muscle myosin II MD bound to the CK-571 inhibitor (blue). The nucleotide is indicated in red sticks. Movie related to Figure 2A in main text.

Movie S2. Sequence differences between Smooth and non-muscle myosin II are far from the CK-571 binding site (based on Figure 2 and S1). Sequence differences between Hs SMM2 and Hs NMM2 are indicated with firebrick colored balls. Note that none of these differences are close to the path or the pocket that the drug will follow or occupy in order to act as an inhibitor.

Movie S3. Comparison of the transducer and the connectors during the recovery stroke. The SM/CK-571 structure shows that the motor domain connectors are not coupled during the recovery stroke and allow the generation of the CK-571 pocket in an intermediate state that has features closer to the PR for the lever arm position and the connector positions, but closer to the PPS for the transducer conformation.

Movie S4. Features of the intermediate state of the recovery stroke stabilized by CK-571. After ATP binding, myosin explores a series of conformations during the recovery stroke. CK-571 binds and stabilizes an intermediate of the recovery stroke revealing how flexible the motor becomes after ATP binding. The CK-571 traps the molecule in a state in which the central beta sheet and the U50 position is closer to that observed in the PPS (black) than that found in Post-rigor (blue). Interestingly however, Switch II is far away from the gamma phosphate position (unlike in the PPS state). Moreover, the lever arm is down, similarly to states close to the post-rigor state (blue). Rotation of the U50 and conformational changes in the seven-stranded central β -sheet are indicated by red arrows. The SM/CK-571 structure reveals that flexibility within the molecule during the recovery stroke allows repriming of the lever arm by repositioning of the SH1 helix and the Relay while the Switch II remains unaffected during the first phase of the recovery stroke.

References (For Supplementary)

1. Sweeney H.L. & Houdusse, A.. Structural and Functional Insights into the Myosin Motor Mechanism, *Annu Rev Biophys.* **39**, 539-57 (2010).
2. Cremo, C.R., Geeves, M.A. Interaction of actin and ADP with the head domain of smooth muscle myosin: implications for strain-dependent ADP release in smooth muscle. *Biochemistry* **37**, 1969-78 (1998).
3. Kovács, M., Wang, F., Hu, A., Zhang, Y. & Sellers, J.R. Functional divergence of human cytoplasmic myosin II: kinetic characterization of the non-muscle IIA isoform. *J. Biol. Chem.* **278**, 38132-40 (2003).
4. Rosenfeld, S.S., Xing, J., Chen, L. & Sweeney, H.L Myosin IIb is unconventionally conventional. *J. Biol. Chem.* **278**, 27449-55 (2003).